A preliminary HVSR investigation of the shallow structure of the Teslin fault, southern Yukon

Daniel O. Afolabi and Hersh Gilbert*
Department of Earth, Energy, and Environment, University of Calgary

Jeremy M. Gosselin
Natural Resources Canada, Geological Survey of Canada–Pacific

Jan Dettmer
Department of Earth, Energy, and Environment, University of Calgary
Yukon Geological Survey

Afolabi, D.O., Gilbert, H., Gosselin, J.M. and Dettmer, J., 2026. A preliminary HVSR investigation of the shallow structure of the Teslin fault, southern Yukon. *In*: Yukon Exploration and Geology 2025, A. Stuart, L.H. Weston and S.K. Schultz (eds.), Yukon Geological Survey, Government of Yukon, p. 75–89.

Abstract

This study investigates the shallow subsurface structure of the Teslin fault zone in southern Yukon using the horizontal-to-vertical spectral ratio (HVSR) method. By recording continuous ambient seismic noise on 5 Hz geophones deployed at over 100 sites across the Teslin and Eastern Teslin faults between July and August 2023, we seek to delineate variations in resonance frequency and amplitude related to geologic and structural features. Data were processed to isolate low-noise intervals, and HVSR curves were calculated to estimate changes in sediment structure, impedance contrasts and near-surface heterogeneities. Our observations reveal distinct spatial variations in HVSR signatures that correlate with mapped terranes and fault strands. Low-frequency, high-amplitude HVSR peaks correspond to a thicker sedimentary layer within fault-bounded basins, whereas high-frequency, low-amplitude responses reflect thin sediment cover over bedrock. Comparisons with Bouguer gravity anomalies indicate consistent spatial correlations between low resonance frequencies and more negative gravity anomalies. These findings demonstrate that the Teslin fault serves as a lithologic and structural boundary, as well as showcases the value of single-station passive-seismic methods for mapping variability in subsurface structure that is masked by sediment overburden. This study provides a foundation for future joint inversions of surface-wave dispersion, gravity, and magnetic data, which will help refine models of shallow seismic properties to better support geothermal assessments in southern Yukon.

Plain language summary

This study investigates regions around the Teslin fault in southern Yukon to better understand the structure of the shallow Earth. The Teslin region is known for its complex geology, where different rock units and past fault movements have created a complex geologic patchwork. This geologic structure influences how water and heat move through the uppermost part of the crust. To explore what lies below the surface, we continuously recorded the natural vibrations of the ground shaking at more than 100 locations during the summer of 2023. These small vibrations, caused by wind, rivers, storms and human activity, travel differently through soft sediments than through solid rock. By examining these vibrations at each site, we were able to estimate changes in the speeds that the ground vibrations travel and variations in the thickness of soils or sediments that overlie bedrock. Our results indicate clear changes in the subsurface that align with known faults and different rock types. The Teslin fault appears to mark a location of changing subsurface structures. Understanding the shallow structure of the Teslin fault and adjacent areas helps identify the pathways of heat and fluid in the shallow subsurface, which is important for geothermal assessment. This study also provides a framework for future, more detailed investigations of the Teslin fault in this region.

* daniel.afolabi@ucalgary.ca

Introduction

Southern Yukon is characterized by a network of crustal-scale faults that exert control on its geology and tectonics. The major fault systems include the Denali, Teslin and Tintina faults which extend to lengths of >2000 km and have accommodated hundreds of kilometres of right-lateral displacement (Fig. 1; Mortensen, 1992; Snyder et al., 2005). Collectively, these faults define major terrane boundaries within the northern Canadian Cordillera and have accommodated accretionary and later Cenozoic deformation (de Keijzer et al., 2000; Fisher et al., 2007; Yukon Geological Survey, 2011). Their long-lived tectonic activity has generated extensive fracture networks, fault gouge, and disrupted stratigraphy, producing the pronounced geologic complexity characteristic of the region (Mortensen, 1992).

Large strike-slip faults, such as the Denali and Teslin, are known to generate broad zones of deformation comprising fractured, altered rock volumes and damage zones (Stevens and Erdmer, 1996; Fisher et al.,

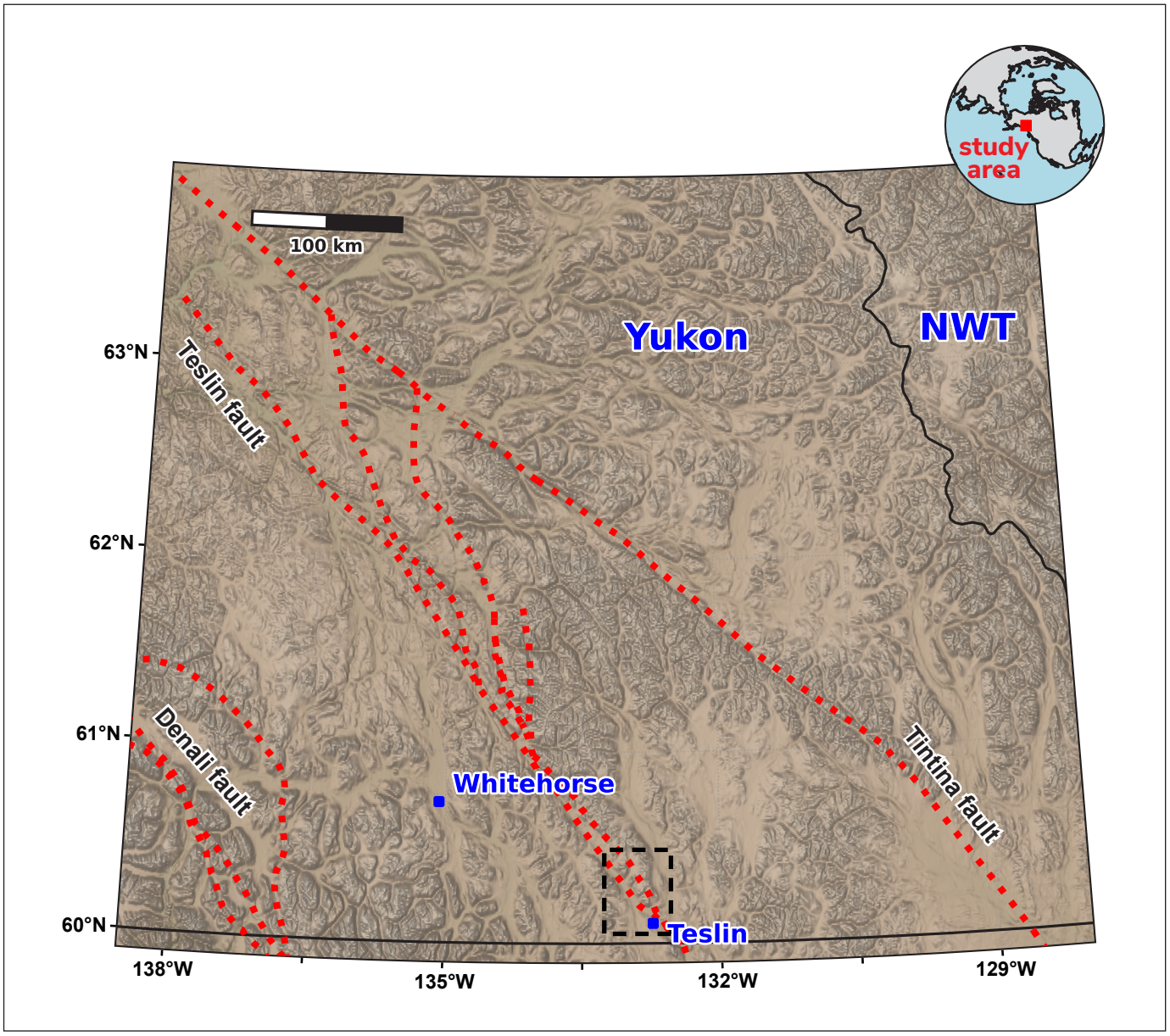

Figure 1. *Map of the Yukon and Northwest Territories (NWT), Canada, indicating the locations of the Denali, Teslin and Tintina faults (red dashed lines). The locations of Whitehorse and Teslin are indicated by blue squares. The inset map indicates the position of the study area in northwestern North America. The black dashed outlined box presents the approximate extent of the study area.*

2007; Witter, 2023). These damage zones can extend hundreds of metres to kilometres from the main fault core, depending on lithology and slip history (Caine et al., 1996; Faulkner et al., 2010). In southern Yukon, such zones are particularly well developed where faults juxtapose contrasting terranes; for example, the Denali fault separating the Kluane schist from Mesozoic sedimentary packages, or the Teslin fault bounding plutonic intrusions against Paleozoic–Mesozoic sediments. The resulting heterogeneity is manifested in variable sediment accumulation, disrupted stratigraphy and complex seismic velocity structures (Gilbert et al., 2006; McDermott et al., 2019; Estève et al., 2021).

The Teslin fault zone in southern Yukon is characterized by the juxtaposition of diverse lithological terranes and the presence of multiple fault strands and subsidiary structural features (Fig. 2; de Keijzer et al., 2000; Larson, 2002; Hayward, 2015). Locally, the fault bifurcates into multiple strands and subsidiary shear zones, incorporating slivers of Quesnellia and Atlin terranes within a structurally intricate duplex system (Larson, 2002; Witter, 2023). This bifurcation has produced localized pull-apart basins and strike-slip duplex structures along the fault zone, representing zones of transtensional deformation that promote intense brittle fracturing, interconnected fracture networks, and enhanced structural permeability (Caine et al., 1996; de Keijzer et al., 2000; Faulkner et al., 2010). Structural depressions such as the Fox Creek trough, interpreted as a fault-related, pull-apart basin infilled with low-density sediments, exemplify this process and may provide pathways for geothermal fluid circulation within the strike-slip duplex system (Witter, 2023). This connectivity has the potential to influence hydrothermal flow and the distribution of geothermal resources within the Teslin fault corridor (Witter, 2023).

Recent geophysical and geologic investigations reveal pronounced lithologic contrasts across the Teslin fault (de Keijzer et al., 2000; Snyder et al., 2005; Hildes, 2022; Witter, 2023). The northeastern domain is underlain by Neoproterozoic to Paleozoic metamorphic rocks of the Yukon-Tanana terrane, primarily quartzite and schist, whereas the southwestern domain consists of Mesozoic chert, shale, carbonate and volcanic rocks of the Cache Creek terrane (Fig. 2; Witter, 2023; Sternbergh and Colpron, 2025). Intrusive bodies, including the Early Cretaceous Deadman Creek pluton (Fig. 2), further diversify the subsurface geology and influence local heat flow.

The interplay between fault-controlled fracture systems, lithologic variability and moderate regional heat flow likely affects the geothermal potential of the Teslin area. Although the Teslin fault is considered tectonically inactive, it preserves a legacy of deformation characterized by fractured and altered rock volumes that may sustain residual structural permeability (Colpron et al., 2021; Witter, 2023). This permeability, combined with the favourable thermal conditions of the region, underscores the potential for geothermal development around the Teslin fault zone. However, the subsurface characterization of the region remains limited due to sparse near-surface geophysical data (de Keijzer et al., 2000; Larson, 2002; Monger and Price, 2002; Fraser et al., 2018; Witter, 2023).

Passive seismic methods, such as the horizontal-to-vertical spectral ratio (HVSR) technique, offer a practical and non-invasive means of imaging shallow geologic structures. The HVSR method uses ambient seismic noise to identify resonance frequencies generated by seismic impedance contrasts, allowing estimation of sediment thickness, bedrock depth and subsurface layering (Lane et al., 2008; Haefner et al., 2011; Stannard and Meyers, 2018). Building on the success of HVSR applications in mapping basin geometry and fault-related structures in other geologic settings (Haefner et al., 2011; Stannard and Meyers, 2018; Berumen-Borrego et al., 2024), this study applies the HVSR technique to data collected along transects crossing the Teslin fault zone as a preliminary step toward addressing existing data gaps.

Specifically, we employ HVSR surveys to delineate spatial variations in the thickness of sedimentary layers and impedance contrasts within the shallow structures surrounding the Teslin fault and its eastern strand. Based on these observations, we explore the continuity of fault-controlled structures and their relationship to the configuration of geologic units. Characterizing these features will contribute to constraining the near-surface architecture and permeability distribution, which is needed for future heat-flow modelling and geothermal assessment. Ultimately, this study seeks to enhance the geologic understanding of the Teslin fault zone and demonstrate the utility of HVSR as a cost-effective tool for early geothermal exploration in structurally complex and data-scarce regions.

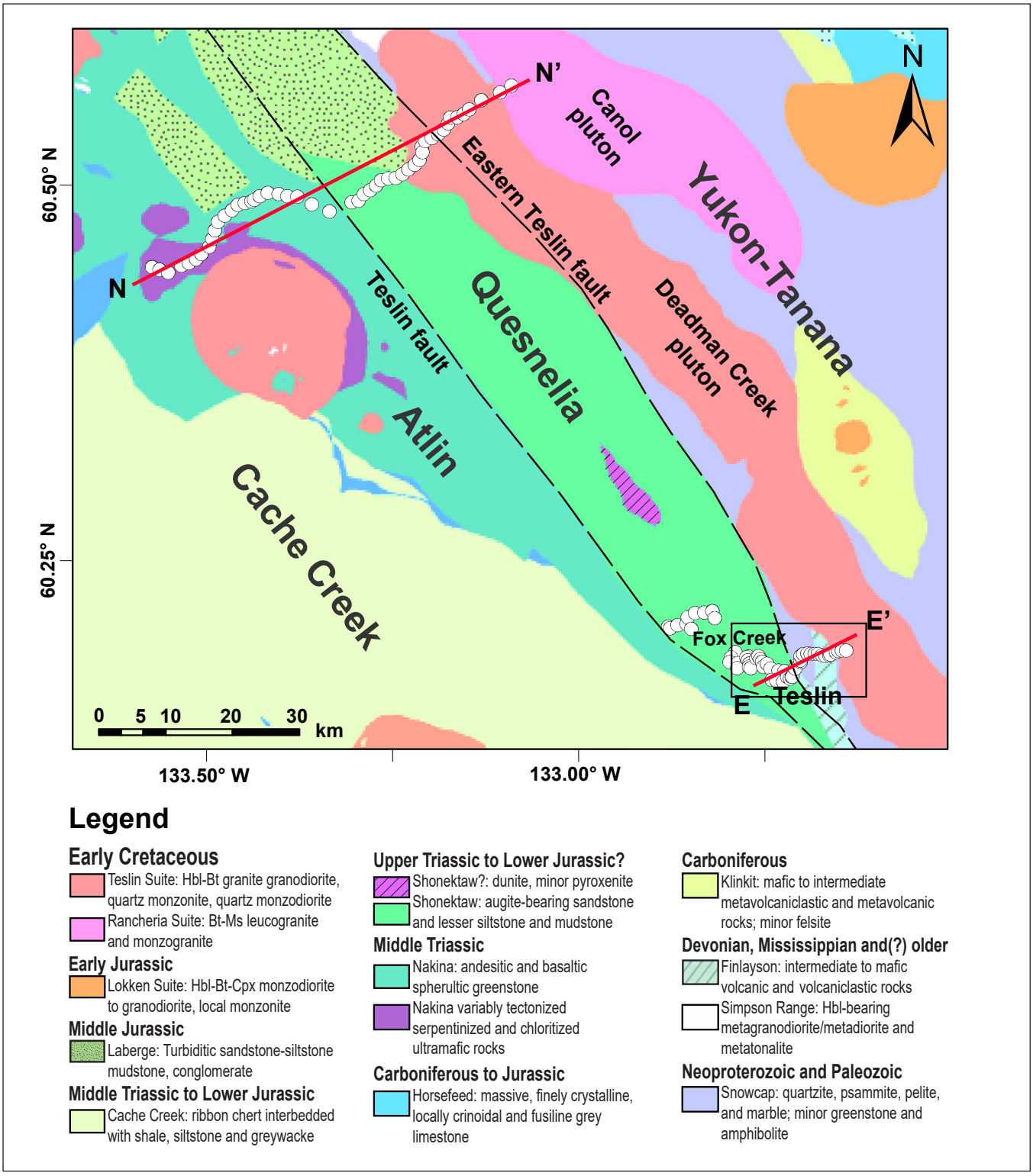

Figure 2. *Geological map (Yukon Geological Survey, 2023) of the Teslin fault near the town of Teslin including locations of the Yukon-Tanana, Quesnellia, Atlin and Cache Creek terranes. Faults are indicated by black dashed lines. Geophone locations are displayed as white circles. Locations of profiles N-N' and E-E' presented in Figures 5 and 6 are displayed as red lines. The box with the black outline represents the area with the available Bouguer anomaly map (presented in Figure 7). Bt – biotite; Cpx – clinopyroxene; Hbl – hornblende; and Ms – muscovite.*

Geologic and tectonic setting of the Teslin fault zone

Southern Yukon, located in the northern Canadian Cordillera, comprises a complex collage of terranes that accreted during the Mesozoic and Cenozoic, including the Yukon-Tanana (YTT), Stikinia, Wrangellia, Quesnellia, Atlin and Cache Creek terranes (Monger and Price, 2002; Colpron et al., 2007, 2022). These terranes are juxtaposed along sharp structural boundaries formed by thrusting, subduction and crustal deformation (Evenchick et al., 2005; Johnston and Canil, 2007). The Teslin fault, a northwest-trending, right-lateral, strike-slip system is a major feature separating key terranes (Colpron et al., 2021; Witter, 2023). The fault zone contains Paleozoic–Mesozoic metavolcanic rocks juxtaposed with Triassic–Jurassic chert and carbonates of the Cache Creek terrane (Yukon Geological Survey, 2011), and records multiple deformation phases, including early sinistral ductile shearing and mylonitization (Early Jurassic–mid-Cretaceous) followed by later dextral transpressional motion (Late Cretaceous–Tertiary; de Keijzer et al., 2000; Larson, 2002). Despite the current low level of activity along the Teslin fault, the structural inheritance and fracture network of the fault zone continue to influence the regional tectonic framework, resource distribution and crustal permeability.

The surficial geology near the Teslin fault consists of variable Quaternary deposits, including till, glaciofluvial sand and gravel, outwash terraces, and colluvial material (Witter, 2023). These sediments overlie faulted bedrock units composed mainly of quartzite, volcanic and meta-intrusive rocks (Denny, 1952; Witter, 2023). The distribution and thickness of sediments are highly irregular due to glacial advance, meltwater reworking and postglacial surface processes. Locally, surficial sediments are stratigraphically complex, which influences interpretations of shallow structure (Morison and Klasen, 1997; Witter, 2023). The observations of HVSR resonant frequencies presented here provide needed constraints for resolving sediment thickness.

Method

Data acquisition

For this study, the HVSR method was used because of its ease in data processing and sensitivity to seismic discontinuities in shallow structure (e.g., Nakamura, 1989, 2008; Cipta et al., 2018; Berumen–Borrego et al., 2024). Continuous seismic data was collected to examine the structure of the Teslin fault zone and surrounding area near the village of Teslin in southern Yukon (Fig. 2). Continuous seismic signals were recorded using the three-component Inova Hawk 5-Hz nodal geophones. Each seismic sensor records three orthogonal components of ground motion (vertical, north–south and east–west) at 250 Hz, allowing flexibility for both microtremor and higher-frequency ambient noise applications. The continuous recordings were made between July and August 2023 at a total of 104 locations in the study area.

Data processing

Using a combination of the open-source Obspy (Beyreuther et al., 2010; Krischer et al., 2015) and HVSRPY Python software (Vantassel et al., 2021, 2023), we processed the continuous three-component raw recordings and performed HVSR measurements. Initially, we processed an entire day of data and found time variable peaks whose amplitudes changed with noise level throughout the day. To improve the reliability of HVSR measurements, only segments of data from the quietest period of each day were retained for further analysis. To find these quiet time windows, we first filtered the continuous recordings between 0.5 and 25 Hz using a four-pole Butterworth bandpass filter. The standard deviation of these filtered waveforms was then calculated using a three-hour, long-moving time window. Following testing shorter and longer time windows, ranging between one hour to an entire day of data, we selected the three-hour window because it produced HVSR curves with clearer peaks, higher amplitudes and fewer spurious peaks. The three-hour long windows with the lowest standard deviation across all three components from each day of recording were used for stacking and further analysis. We found the quiet period varied from day to day and occurred mostly during the middle of the night local time. This time windowing approach reduced the influence of temporally varying signals and spurious noise.

The HVSRPY workflow provides a reproducible, and standardized framework that complies with the SESAME (2004) recommendations for ambient-noise spectral ratio estimation (Cox et al., 2020). Further details of the data processing and window selection/rejection can be found in the description of HVSRPY (Cox et al., 2020; Vantassel et al., 2023). The initial steps of HVSRPY processing remove linear trends from the quiet three-hour segments and cut the timeseries into 100-second windows. A cosine (Tukey) taper with

a 10% width was applied to the start and end of each window to suppress edge-related spectral leakage (Konno and Ohmachi, 1998). The HVSR calculations followed the method described by Nakamura (1989) as implemented within HVSRPY in which each time window was transformed into the frequency domain using a fast Fourier transform. To reduce spectral variability and highlight dominant resonance behaviour, the resulting curves were smoothed using the logarithmic Konno-Ohmachi filter with a bandwidth coefficient b=40 (Konno and Ohmachi, 1998). The stacked HVSR curves and peak resonant frequencies presented here for each station are calculated based on the average values of the HVSR curves from the quiet hours (i.e., lowest noise variance) determined for each day. The lowest-frequency peaks on each HVSR curve are automatically identified using an algorithm that selects the fundamental resonant frequency (f_0) with sufficiently high amplitude. These f_0 peaks are interpreted to represent the primary impedance contrast associated with the thickness and velocity of sediments overlying bedrock. Because f_0 is controlled by both the thickness of the sedimentary layer and their average shear wave velocity, there are tradeoffs interpreting HVSR in terms of either parameter (Fig. 3). For example, low frequency HVSR peaks can result from the layers overlying bedrock either being thick or comprised of material with low shear wave velocities. Conversely, thin layers or layers comprised of high velocity material can contribute to high-frequency HVSR peaks.

Interpreting HVSR curves are inherently non-unique. Different subsurface structures can yield identical Rayleigh-wave ellipticity or spectral ratio signatures (Hobiger et al., 2013). Consequently, and in line with recommendations from recent sensitivity analyses (SESAME, 2004), we limit our interpretation to comparing relative changes in HVSR between stations rather than attempting to derive absolute models. In this study, variations in f_0 are evaluated in terms of their spatial patterns and are compared with Bouguer gravity anomalies to produce geologic interpretations.

Results

All the stations that we operated around Teslin were fully analyzed. We present HVSR curves for a subset of 37 sites from the Teslin survey to demonstrate changes in signal along two transects crossing the Teslin fault zone. The selected sites are representative of the full dataset and capture the range of HVSR responses and key structural variations. The selected HVSR curves presented here clearly demonstrate changes in site response across the study area. We also present the resonant frequencies for another 27 sites to compare with structures along the southern transect. The HVSR curves display clear peaks related to their fundamental resonant frequencies that range between 0.28 and 28 Hz, reflecting the changing and heterogenous structures around the Teslin fault. Viewing examples of HVSR spectrograms calculated for the continuous data recorded at two of the stations used here (E03 and N30) displays time variable signals that correlate with meteorological conditions (air temperature and wind speed) in Teslin (Fig. 4). Temperature and wind speed display strong diurnal variations throughout the observation period. Daily maximum temperatures reach

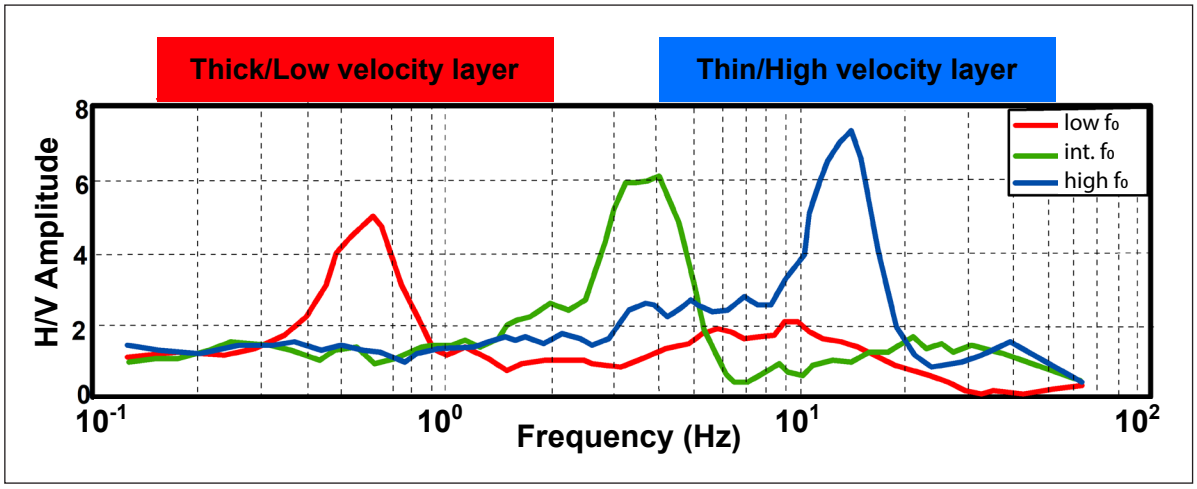

Figure 3. *Schematic illustration of HVSR measurements demonstrating the relationship between resonant frequencies (low – red, intermediate – green, high – blue), seismic wavespeeds and sediment thickness.*

approximately 25–28°C, while minimum temperatures drop to near ~5–10°C, consistent with daily cycles during the summer. Average daily wind speeds fluctuate around ~5–10 km/h with occasional short bursts exceeding 20 km/h. The HVSR spectrograms display distinct peaks that exhibit daily fluctuations in amplitude and peak frequencies. At station E03, two persistent peaks are observed at frequencies between 1.5–2.5 Hz and near 9 Hz (Fig. 4a). The high-frequency component exhibits a periodic pattern, with amplitude alternating between higher and lower values over the observation period. The HVSR amplitude for E03 is greatest in the 1.0–2.5 Hz range and displays consistent daily variation. A secondary pulse between 7 and 9 Hz also displays daily amplitude fluctuations, though with lower amplitude than the primary low-frequency peak. At station N30, a strong HVSR signal is observed between 2 and 3 Hz, with amplitudes ranging from approximately 3.5 to 5 (Fig. 4b). This signal also indicates daily variations in amplitude, like the pattern observed at E03. The recurring diurnal fluctuations in both stations indicate that the HVSR response varies over time, with clear frequency-dependent differences in amplitude stability and persistence. Despite these hourly variations in HVSR signals that appear to result from environmental effects on the ambient seismic noise wavefield, the spectrograms reveal that the peaks in resonant frequencies are consistent throughout the recording period. Further analysis presented below is based on average HVSR curves taken from the mean of the signal attained from the quiet recording period each day, which enables more reliable comparability between measurements from different sites.

Our analysis focuses on two profiles that transect the main traces of the Teslin fault and the Eastern Teslin fault. The HVSR results along profile N–N' are presented in Figure 5, and Figure 6 presents the corresponding results for the E–E' profile. These profiles provide coverage across zones of contrasting lithology and fault geometry, whereas facilitates analysis of site response across the fault. For each profile, the amplitudes of HVSR curves are plotted at the same scale, so relative amplitudes of the signals can be compared. The N–N' profile, with a length of nearly 38 km, spans the Teslin fault (TF) and samples the Nakina Formation (NK) at its

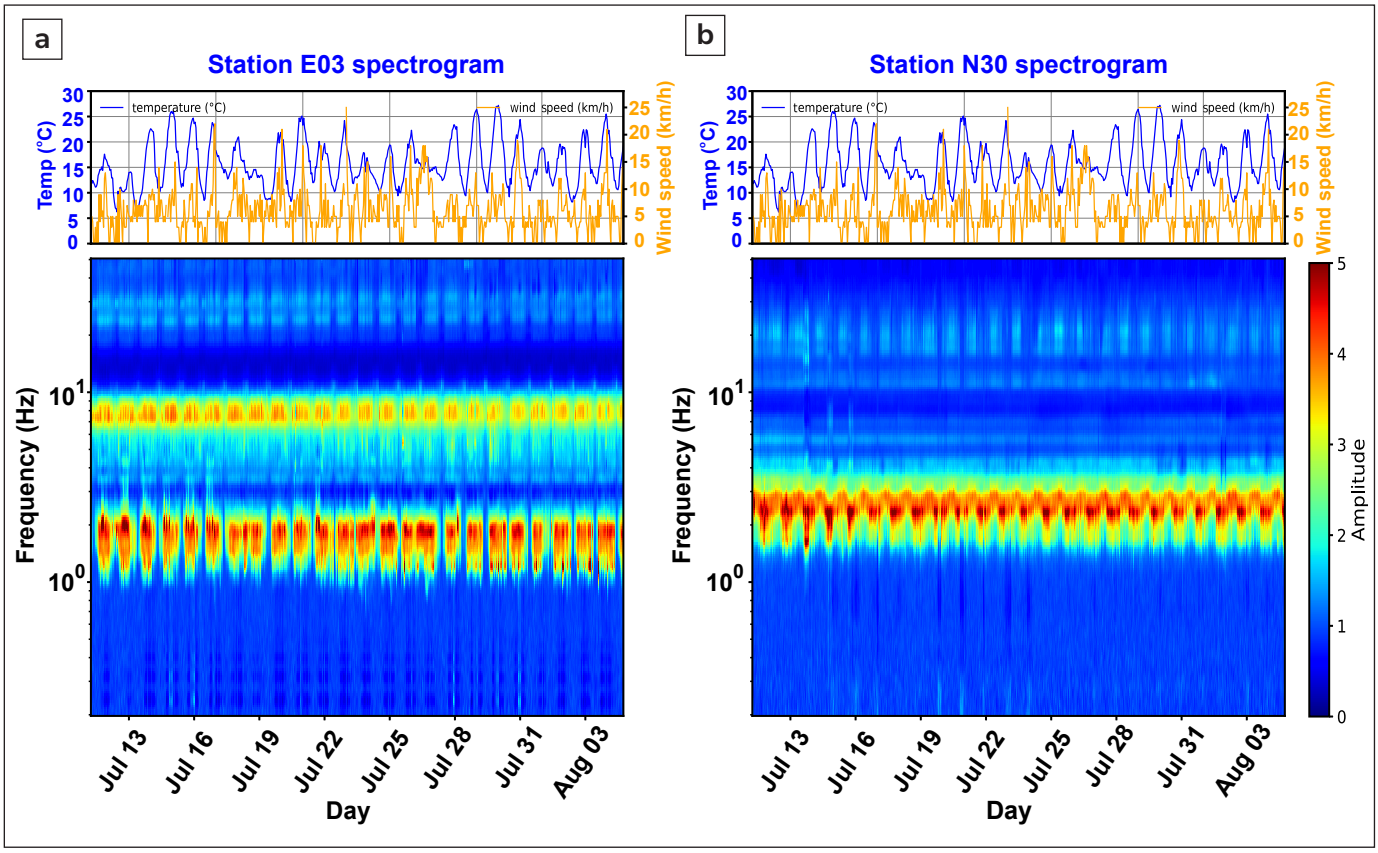

Figure 4. *Environmental conditions and HVSR variability at sites* ***(a)*** *N30 and* ***(b)*** *E03. Top panels illustrate temperature and wind speed. Bottom panels display a spectrogram depicting temporal variations of HVSR signals between July 11 and August 5, 2023. The weather data was downloaded from Environment and Climate Change, Canada for the Teslin area, Yukon.*

southwestern end. Its central segment extends across the Shonektaw formation (ST) and the Teslin suite (TS), and ends at the Canol pluton (CP) to the northeast. Profile E–E' extends for ~7 km and crosses the Eastern Teslin fault from the Shonektaw formation (ST) in the west, to multiple geologic blocks associated with the Finlayson (FN) and Snowcap (SC) assemblages, as well as the Teslin suite (TS) in the east.

Topography along profile N–N' rises from ~750 m in the southwest to ~1450 m in the northeast (Fig. 5a). Elevations remain subdued (750–900 m) across the low-relief Nakina Formation, then dip slightly near the Teslin fault. Farther east, the terrain steepens across the Shonektaw formation and Teslin suite, reaching >1100 m near the Eastern Teslin fault. The highest relief occurs in the northeast, where elevations sharply exceed 1300 m over the Canol pluton. The surface elevations exhibit moderate relief, with localized depressions and ridges located close to mapped fault zones, particularly near the Teslin fault and between geologic units (Fig. 5a). The HVSR profile illustrates the spatial variation in the stacked HVSR curves including the frequencies and amplitudes of their peaks (Fig. 5b). Southwest of the Teslin fault, stations between horizontal offsets of 0 and 7 km, are located within the tectonized portion of the Nakina Formation and display HVSR curves with double or multiple peaks, and peak resonant frequencies between 0.6 and 2 Hz. This part of the transect possesses moderate topographic relief. Between horizontal offsets of 7 and 18 km along this profile, the HVSR peaks shift to higher frequencies while maintaining multi-peaked spectra. Resonant frequencies increase from 0.6 Hz in the eastern part of the andesitic and basaltic Nakina Formation to ~2 Hz west of the Teslin fault where f_0 deceases to ~1 Hz at the fault. The lack of large variations in resonant frequency among stations within this region of the Nakina Formation suggests laterally consistent seismic response and that the area only exhibits modest structural variations.

Stations farther to the east between horizontal offsets of 18 and 23 km, spanning the Teslin and Eastern Teslin faults, are located within the Shonektaw formation and exhibit some of the highest amplitude HVSR curves observed in this study. The HVSR curves within this interval exhibit single, well-defined peaks with resonant frequencies ranging between 1 and 3 Hz. Compared with the lower-frequency, multi-peaked responses southwest of the Teslin fault, this section displays higher and more uniform resonant frequencies. Along sections of the profile east of offsets of 25 km, the resonant frequencies increase gradually to the northeast, accompanied by an increase in amplitude. Northeast of the Eastern Teslin fault, between 23 and 38 km, the HVSR curves display multiple frequency peaks. The spectra in this region are dominated by higher-frequency peaks between ~3.5 and 15 Hz with resonant frequencies that increase to the northeast, within the Deadman Creek pluton of the Teslin suite, and the Canol pluton (Fig. 5c). A change in f_0 occurs at the Eastern Teslin fault within the Teslin suite at a horizontal offset ~27 km.

The topography along profile E–E' is lower than that found along N-N' and ranges from ~690 to 760 m (Fig. 6a). Elevations remain near ~700 m across the Shonektaw formation, with a small depression at the Eastern Teslin fault followed by a modest rise to ~730 m over the Finlayson and Snowcap assemblages. The topography reaches its maximum elevation within the Deadman Creek pluton of the Teslin suite, along this profile. The stacked HVSR curves along the E–E' transect (Fig. 6b) display clear variations in amplitude, shape, and resonant frequency across the 7 km profile. In the southwestern segment of the line, between horizontal offsets of 0 and 2.2 km within the Shonektaw formation, the curves exhibit multiple broad peaks with f_0 values of ~1.5–2.2 Hz. The stations within this unit display high HVSR amplitudes with only subtle shifts in peak frequencies. Where the profile intersects the Finlayson assemblage, between horizontal offsets of ~2.2 and 2.5 km, the HVSR signals exhibit reduced amplitudes compared to the Shonektaw formation (Fig. 6c). The HVSR peaks in the Finlayson assemblage are narrower, and the curves indicate less variability in their frequency content. Between horizontal offsets of ~2.5 to 4 km across the Snowcap assemblage, the HVSR curves shift to a single peak with resonant frequencies between ~3.5 and 10 Hz. The HVSR signals within the Snowcap assemblage possess reduced amplitudes compared to those sampling other units (Fig. 6b). Returning to sampling the Finlayson assemblage between horizontal offsets of ~4 to 5.3 km, the HVSR peaks shift to lower frequencies and have a single peak from 1.3 to 2 Hz. In the easternmost segment of the profile, spanning horizontal offsets of approximately 5.3 to 7 km, where stations cross from the Snowcap assemblage into the Teslin suite (Fig. 6c), the HVSR curves vary in peak frequency and amplitude. Resonant frequencies increase from ~2 to ~3.5 Hz and HVSR curves possess multiple peaks.

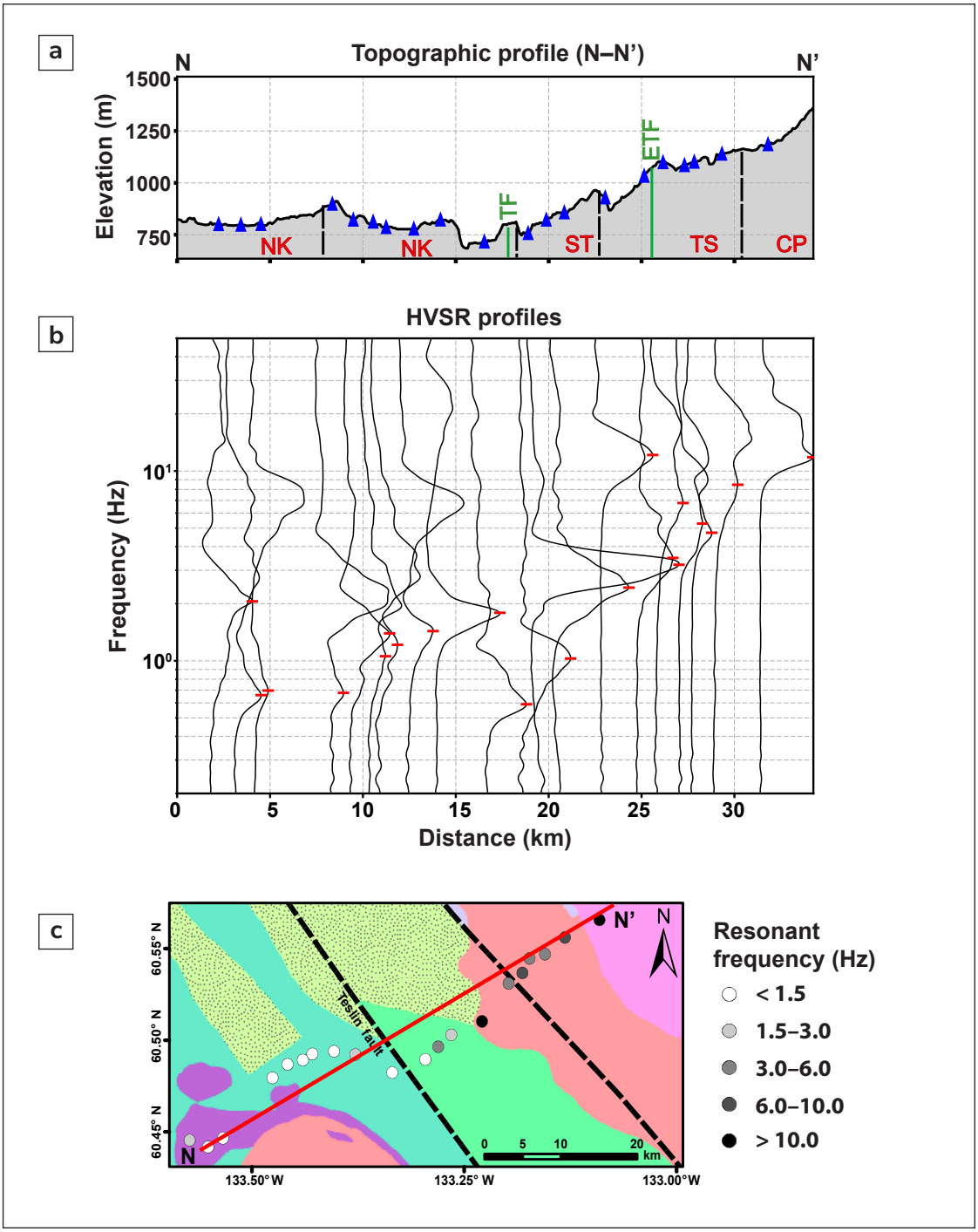

Figure 5. *Horizontal-to-vertical spectral ratio (HVSR) results along the N–N' transect.* ***(a)*** *Topographic profile along the transect. Geophone locations are indicated by blue triangles. Locations of fault surface traces are indicated by green lines. TF – Teslin fault; ETF – Eastern Teslin fault. Boundaries between mapped geologic units are depicted as dashed lines. Geologic units are labeled: western part of the Nakina Formation (NK) consists of variably tectonized serpentinized and chloritized ultramafic rocks, and to the east, consists of andesitic and basaltic spherulitic greenstone; ST – Shonektaw formation; TS – Teslin suite; CP – Canol pluton.* ***(b)*** *HVSR curves for geophones along transect N–N'. The red lines on the HVSR profile represent the measured resonant frequency of the site.* ***(c)*** *Geologic map illustrating the stations in the northern transect of the Teslin fault project on profile N–N'. Geophone locations are displayed as circles, coloured according to measured resonant frequency. Fault traces are indicated by dashed lines and are labeled. See legend of geologic units in Figure 2.*

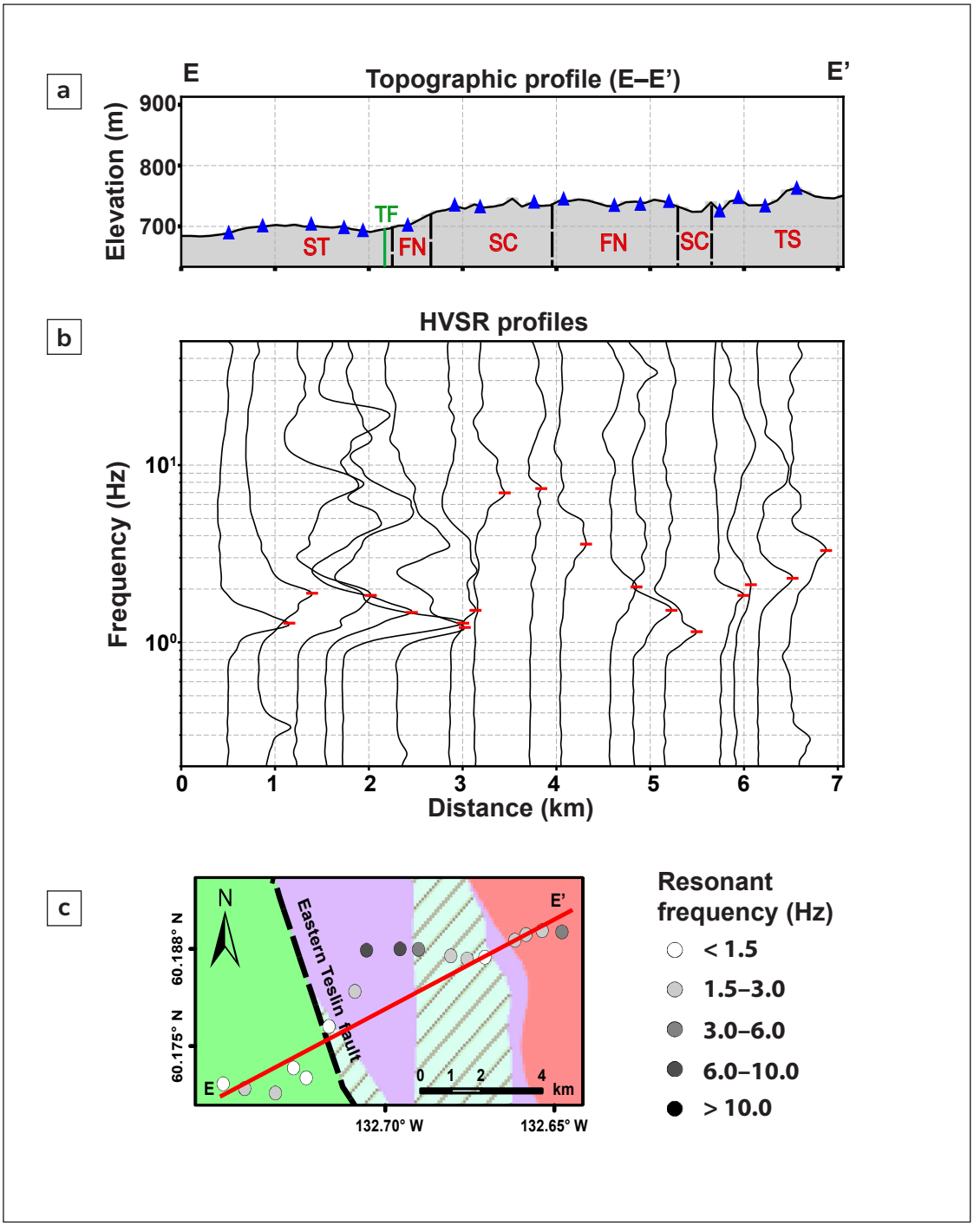

Figure 6. *Horizontal-to-vertical spectral ratio (HVSR) results along the E–E' transect. Details as in Figure 5. Geologic units are labeled: ST – Shonektaw formation; FN – Finlayson assemblage; SC – Snowcap assemblage; TS – Teslin suite. See legend of geologic units in Figure 2.*

Discussion

Implications for boundaries in bedrock geology

Horizontal-to-vertical spectral ratio (HVSR) observations across a broad region surrounding the Teslin fault and its surrounding area reveal several consistent patterns. We find that the locations of changes in HVSR curves and peak frequencies observed here display similarities between the locations of faults and geologic units around the Teslin fault in southern Yukon. The characteristics of the HVSR curves including the amplitude and widths of HVSR peaks, the frequencies of those peaks, and whether the curves possess single or multiple peaks, all appears to vary between geologic units. Lithologic transitions between geologic units are accompanied by changes in HVSR signature, which suggests that changes in bedrock units, and the contrasting seismic properties between the bedrock units and their overlying layers, contribute to the observed HVSR signatures.

The HVSR curves from sites sampling the Nakina Formation on the western segment of the N–N' transect (offsets <18 km; Fig. 5b), display broad peaks with increasing amplitudes from <1 Hz up to 7–8 Hz. The systematic increase in HVSR peak amplitudes from the tectonized ultramafic Nakina Formation in the west, to the andesitic and basaltic Nakina Formation in the east toward the centre of the transect indicates that variations in bedrock lithology accompany changes in contrasting seismic properties between the bedrock and overlying sediments. In this context, the greater HVSR peak amplitudes in the central part of the transect suggests that the difference in seismic properties between the underlying bedrock and surficial deposits is greater than that found for the units to the west.

Sites within the Shonektaw formation of the Quesnellia terrane possess the highest amplitude HVSR peaks along both the N–N' and E–E' profiles (Figs. 5b and 6b). The large seismic contrast between bedrock within the Shonektaw formation, comprised of sandstone, siltstone and mudstone, and the overlying sedimentary layers can be inferred from the strong HVSR peaks displayed in the central part of N–N' and the western end of E–E'. Isolating the factors responsible for the increased impedance contrast within the Shonektaw formation will require further analysis and modelling. The observations presented here indicate that the history of deformation that shaped the region bound by the Teslin and Eastern Teslin faults has imparted the geologic blocks with a distinct structural signature. Additionally, crustal-scale seismic observations from the SNORCLE lines have been interpreted to indicate that parts of Quesnellia have been thrust onto the Stikinia terrane (e.g., Evenchich et al., 2005). Such episodes of terrane overthrusting would produce intracrustal seismic discontinuities and impart signatures of deformation.

The HVSR curves for the stations sampling the Teslin suite, on the eastern sides of both the N–N' and E–E' profiles, exhibit broad peaks that extend from 2 Hz to as high as 10 Hz or greater (Figs. 5c and 6c). The structural configuration responsible for HVSR peaks at high frequencies could be a shallow layer that is either thin or characterized by low seismic velocities (Fig. 4). A thin layer of sediments fits expectations for the area of the Teslin suite at high elevations above 1 km sampled along N–N'. Further modelling will be necessary to constrain the source of broad peaks that extend to high frequencies within the area of the Teslin suite along E–E' at lower elevations.

HVSR and Bouguer gravity anomalies

In addition to the HVSR changes that align with changes in geology and fault locations, the spatial distribution of HVSR derived resonant frequencies follows a similar trend to the distribution of Bouguer gravity anomalies. Our sampling along the E–E' profile and other stations near Teslin are located within the area of a recent gravity survey (Figs. 2 and 7; Witter, 2023). Stations characterized by low-resonant frequencies (<1.5 Hz), are located within regions of more negative Bouguer anomalies (Fig. 7). Conversely, higher–frequency responses (6–28 Hz) are concentrated in regions characterized by less negative Bouguer gravity anomalies (Fig. 7). The pattern of resonant frequencies follows a trend in which higher frequencies coincide with the locations of gravity highs on either side of the Eastern Teslin fault (Fig. 7). Closer to the fault, we observe resonant frequencies decrease to lower values as Bouguer anomaly values decrease to more negative values. The similar patterns in Bouguer anomalies and resonant frequencies highlight the complimentary nature of these datasets in delineating basin geometry, sediment fill, and near-surface structural variability, particularly across complex zones such as the Teslin fault. Additionally, the observed coincidence of gravity anomalies with HVSR signatures suggests they are influenced by common structural sources such as the distribution of faults and changes in the thickness of shallow sedimentary cover.

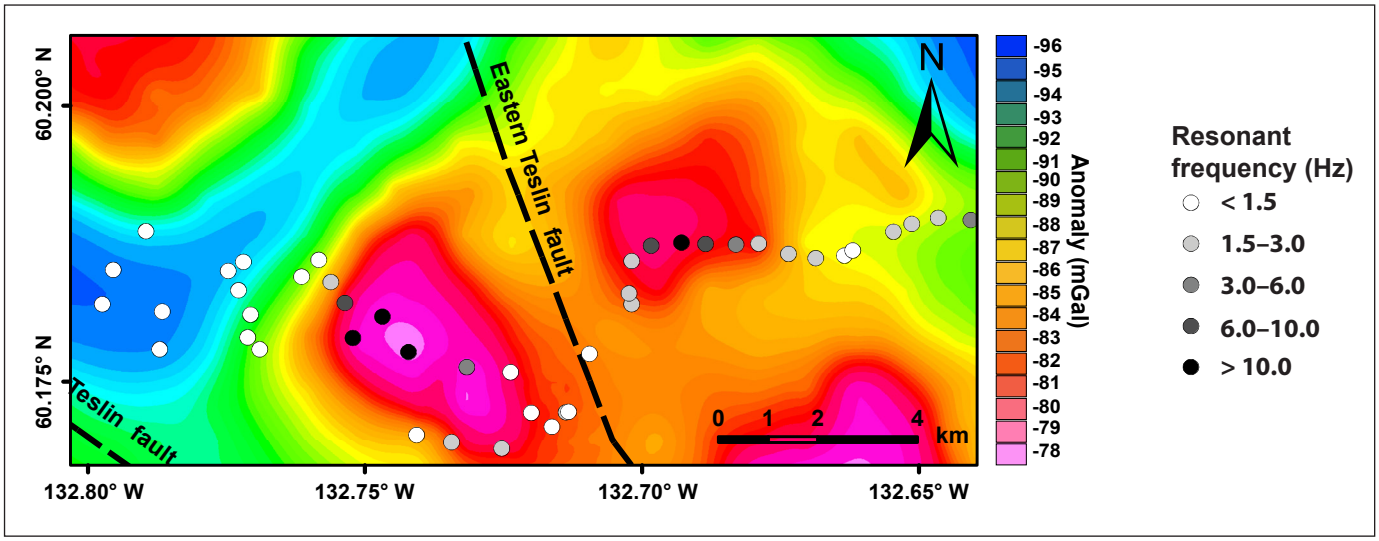

Figure 7. *Comparison between Bouguer gravity anomaly and HVSR measurements. Bouguer gravity anomaly map is modified from Witter (2023). Circles denote geophone locations, coloured according to measured resonant frequency. Fault traces are indicated by black dashed lines and are labeled.*

Conclusions

The HVSR investigation across the Teslin fault zone provides new insights into its shallow architecture. The results reveal distinct spatial variations in resonant frequency and amplitude that correlate with mapped geologic units, fault strands and topographic features. These observations delineate the Teslin and Eastern Teslin faults as structural boundaries separating zones of contrasting subsurface seismic properties. Identifying similar patterns in resonance frequencies and Bouguer anomalies points to the sensitivity of both sets of observations to the same subsurface structures. In summary, these preliminary results find that the Teslin fault and its surrounding features serve as lithologic and structural boundaries that influence the distribution of sediment thickness and contrasting seismic properties. Future work will focus on formal, joint inversion of multiple geophysical data types to create detailed models of the subsurface for future geothermal exploration.

Acknowledgments

We extend our gratitude to the Teslin Tlingit Council for allowing us to conduct field measurements on their land. We also acknowledge the financial support from the University of Calgary, Yukon Geological Survey, and from the Natural Sciences and Engineering Research Council of Canada through Alliance Grant ALLRP-580887-22 and Discovery Grants awarded to Hersh Gilbert and Jan Dettmer. A constructive critical review by Collin Paul helped improve this report.

References

Berumen-Borrego, F., Gilbert, H., Dettmer, J., Gosselin, J.M. and Shahsavari P., 2024. Shear-wave velocities from broadband HVSR measurements for geothermal resource assessment near Burwash Landing, Yukon. *In:* Yukon Exploration and Geology 2023, L.H. Weston and Purple Rock Inc. (eds.), Yukon Geological Survey, p. 1–15.

Beyreuther, M., Barsch, R., Krischer, L., Megies, T., Behr, Y. and Wassermann, J., 2010. ObsPy: A python toolbox for seismology. Seismological Research Letters, vol. 81, no. 3, p. 530–533, https://doi.org/10.1785/gssrl.81.3.530.

Caine, J.S., Evans, J.P. and Forster, C., 1996. Fault zone architecture and permeability structure. Geology. vol. 24, no. 11, p. 1025–1028, https://doi.org/10.1130/0091-7613(1996)024<1025:FZAAPS>2.3.CO;2.

Cipta, A., Cummins, P., Dettmer, J., Saygin, E., Irsyam, M., Rudyanto, A. and Murjaya, J., 2018. Seismic velocity structure of the Jakarta Basin, Indonesia, using trans-dimensional Bayesian inversion of horizontal-to-vertical spectral ratios. Geophysical Journal International, vol. 215, no. 1, p. 431–449, https://doi.org/10.1093/gji/ggy289.

Colpron, M., Nelson, J.L. and Murphy, D.C., 2007. Northern Cordilleran terranes and their interactions through time. GSA Today, vol. 17, no. 4–5, p. 4–10, https://doi.org/10.1130/GSAT01704-5A.1.

Colpron, M., Hayward, N. and Crowley, J.L., 2021. Potential heat production from the Seagull and Teslin plutonic suites, southern Yukon: Geochemistry, geochronology, rock physical properties, and 3D geophysical inversion of Bouguer gravity data. *In:* Yukon Exploration and Geology 2020, K.E. MacFarlane (ed.), Yukon Geological Survey, p.47–72.

Colpron, M., Sack, P.J., Crowley, J.L., Beranek, L.P. and Allan, M.M., 2022. Late Triassic to Jurassic magmatic and tectonic evolution of the Intermontane terranes in Yukon, Northern Canadian Cordillera: Transition from arc to syn-collisional magmatism and post-collisional lithospheric delamination. Tectonics, vol. 41, no. 2, p. 1–32, https://doi.org/10.1029/2021TC007060.

Cox, B.R., Cheng, T., Vantassel, J.P. and Manuel, L., 2020. A statistical representation and frequency-domain window-rejection algorithm for single-station HVSR measurements. Geophysical Journal International, vol. 221, no. 3, p. 2170–2183, https://doi.org.10.1093/gji/ggaa119.

de Keijzer, M., Mihalynuk, M.G. and Johnston, S.T., 2000. Structural investigation of an exposure of the Teslin fault, northwestern British Columbia. Geological Survey of Canada, Natural Resources Canada, Current Research 2000-A5, p. 1–10.

Denny, C.S., 1952. Late Quaternary geology and frost phenomena along the Alaska Highway, Teslin Lake to Whitehorse, Yukon Territory. U.S. Geological Survey Bulletin, 983–C, p. 73–118.

Environment and Climate Change Canada, n.d. Historical Data Climate. Government of Canada, https://climate.weather.gc.ca/historical_data/search_historic_data_stations_e.

Estève, C., Gosselin, J.M., Audet, P., Schaeffer, A.J., Schutt, D.L. and Aster, R.C., 2021. Surface-wave tomography of the northern Canadian Cordillera using earthquake Rayleigh wave group velocities. Journal of Geophysical Research: Solid Earth, vol. 126, no. 8, p. 1–22, https://doi.org/10.1029/2021JB021960.

Evenchick, C.A., Gabrielse, H. and Snyder, D.B., 2005. Crustal structure and lithology of the northern Canadian Cordillera: alternative interpretations of SNORCLE seismic reflection lines 2a and 2b. Canadian Journal of Earth Sciences, vol. 42, p. 1149–1161.

Faulkner, D.R., Jackson, C.A.L., Lunn, R.J., Schlische, R.W., Shipton, Z.K., Wibberley, C.A.J. and Withjack, M.O., 2010. A review of recent developments concerning the structure, mechanics and fluid flow properties of fault zones. Journal of Structural Geology, vol. 32, no. 11, p. 1557–1575, https://doi.org/10.1016/j.jsg.2010.06.009.

Fisher, M.A., Pellerin, L., Nokleberg, W.J., Ratchkovski, N.A. and Glen, J.M.G., 2007. Crustal structure of the Alaska Range orogen and Denali fault along the Richardson Highway. *In:* Tectonic growth of a collisional continental margin: Crustal evolution of southern Alaska, K.D. Ridgway, J.M. Trop, J.M.G. Glen and J.M. O'Neill (eds.), Geological Society of America Special Paper, https://doi.org/10.1130/2007.2431(03).

Fraser, T.A., Grasby, S.E., Witter, J.B., Colpron, M. and Relf, C., 2018. Geothermal studies in Yukon–Collaborative efforts to understand ground temperature in the Canadian North. Geothermal Resources Council Transactions, vol. 43, p. 891–903.

Gilbert, R., Desloges, J.R., Lamoureux, S.F., Serink, A. and Hodder, K.R., 2006. The geomorphic and paleoenvironmental record in the sediments of Atlin Lake, northern British Columbia. Geomorphology, vol. 79, no. 1-2, p. 130-142, https://doi.org/10.1016/j.geomorph.2005.09.021.

Haefner, R.J., Sheets, R.A. and Andrews, R.E., 2011. Evaluation of the horizontal-to-vertical spectral ratio (HVSR) seismic method to determine sediment thickness in the vicinity of the South Well Field, Franklin County, Ohio. Ohio Journal of Science, vol. 110, no. 4, p. 77–85.

Hayward, N., 2015. Geophysical investigation and reconstruction of lithospheric structure and its control on geology, structure, and mineralization in the Cordillera of northern Canada and eastern Alaska. Tectonics, vol. 34, no. 10, p. 2165–2189, https://doi.org/10.1002/2015TC003871.

Hildes, D., 2022. YGS-20221024 Logistic Report on Teslin area gravity survey. YGS-20221024 logistic report prepared by Aurora Geosciences Ltd., Yukon Geological Survey, Submitted October 22, 2022, 266 p.

Hobiger, M., Cornou, C., Wathelet, M., Di Giulio, G., Knapmeyer-Endrun, B., Renalier, F., Bard, P.-Y., Savvaidis, A., Hailemikael, S., Le, B.N., Ohrnberger, M. and Theodoulidis, N., 2013. Ground structure imaging by inversions of Rayleigh wave ellipticity: Sensitivity analysis and application to European strong-motion sites. Geophysical Journal International, vol. 192, no. 1, p. 207–229, https://doi.org/10.1093/gji/ggs005.

Johnston, S.T. and Canil, D., 2007. Crustal architecture of southwestern Yukon and implications for Cordilleran terrane accretion. Tectonics, vol. 26, no. 2, p. 1–18, https://doi.org/10.1029/2006TC001950.

Konno, K. and Ohmachi, T., 1998. Ground-motion characteristics estimated from spectral ratio between horizontal and vertical components of microtremor. Bulletin of the Seismological Society of America, vol. 88, p. 228–241, https://doi.org/10.1785/BSSA0880010228.

Krischer, L., Megies, T., Barsch, R., Beyreuther, M., Lecocq, T., Caudron, C. and Wassermann, J., 2015. ObsPy: A bridge for seismology into the scientific Python ecosystem. Computational Science and Discovery, vol. 8, no. 1, p. 1–17, https://doi.org/10.1088/1749-4699/8/1/014003.

Lane, J.W., Jr., White, E.A., Steele, G.V. and Cannia, J.C., 2008. Estimation of bedrock depth using the horizontal-to-vertical (H/V) ambient-noise seismic method. *In:* Symposium on the Application of Geophysics to Engineering and Environmental Problems, April 6–10, 2008, Philadelphia, Pennsylvania, Proceedings: Denver, Colorado, Environmental and Engineering Geophysical Society, 13 p.

Larson, K.P., 2002. Microstructural analysis of the Teslin fault, northern Canadian Cordillera. British Columbia Geological Survey, Geological Fieldwork 2001, Paper 2002-1, 3 p.

McDermott, R.G., Ault, A.K., Caine, J.S. and Thomson, S.N., 2019. Thermotectonic history of the Kluane Ranges and evolution of the eastern Denali fault zone in southwestern Yukon, Canada. Tectonics, vol. 38, no. 8, p. 2983–3010, https://doi.org/10.1029/2019TC005545.

Monger, J.W.H. and Price, R.A., 2002. The Canadian Cordillera: Geology and tectonic evolution. CSEG Recorder, vol. 27, no. 2, p. 17–36.

Morison, S.R. and Klassen, R.W., 1997. Surficial geology, Teslin, Yukon Territory, Geological Survey of Canada, Open File Map 1891A, scale 1:125 000.

Mortensen, J.K., 1992. Pre-mid-Mesozoic tectonic evolution of the Yukon-Tanana terrane, Yukon and Alaska. Tectonics, vol. 11, p. 836–853, https://doi.org/10.1029/91TC01169.

Nakamura, Y., 1989. A method for dynamic characteristics estimation of subsurface using microtremor on the ground surface. Railway Technical Research Institute, Quarterly Reports, vol. 30, no. 1, https://trid.trb.org/view/294184.

Nakamura, Y., 2008. On the H/V spectrum. The 14th World Conference on Earthquake Engineering, Beijing, China, October 12–17, 2008.

SESAME, 2004. Guidelines for the implementation of the H/V spectral ratio technique on ambient vibrations: Measurements, processing and interpretation. SESAME European Research Project WP12, p. 1–62.

Snyder, D.B., Roberts, B.J. and Gordey, S.P., 2005. Contrasting seismic characteristics of three major faults in northwestern Canada. Canadian Journal of Earth Sciences, vol. 42, no. 7, p. 1223–1237, https://doi.org/10.1139/e05-0276.

Stannard, D. and Meyers, J., 2018. Near surface passive seismic HVSR surveying for mineral exploration, regolith mapping and other applications. *In*: EAGE–HAGI 1st Asia Pacific Meeting on Near Surface Geoscience & Engineering, Yogyakarta, Indonesia, April 9–13, 2018, Program with Abstracts, vol. S401, p. 1–6, https://doi.org/10.3997/2214-4609.201800392.

Sternbergh, S. and Colpron, M., 2025. Summary of geothermal indicators in the Yukon. Yukon Geological Survey, Government of Yukon, Open File 2025-7, 92 p. plus appendices.

Stevens, R.A. and Erdmer, P., 1996. Structural divergence and transpression in the Teslin tectonic zone, southern Yukon Territory. Tectonics, vol. 15, no. 6, p. 1342–1363, https://doi.org/10.1029/96TC01134.

Vantassel, J.P., Cox, B.R. and Brannon, D.M., 2021. HVSRweb: An open-source, web-based application for horizontal-to-vertical spectral ratio processing. International Foundation Congress and Equipment Expo 2021, p. 1–10, https://doi.org/10.1061/9780784483428.005.

Vantassel, J.P., Stolte, A.C., Wotherspoon, L.M. and Cox, B.R., 2023. AutoHVSR: A machine-learning-supported algorithm for the fully-automated processing of horizontal-to-vertical spectral ratio measurements. ArXiv, 25 p., https://arxiv.org/abs/2304.05559.

Witter, J.B., 2023. Analysis of geoscience data for geothermal exploration along the Teslin fault near Teslin, Yukon. Yukon Geological Survey, Government of Yukon, Open File 2023-3, 48 p.

Yukon Geological Survey, 2011. A digital atlas of terranes for the northern Cordillera. Yukon Geological Survey, http://data.geology.gov.yk.ca/Compilation/2, [accessed 15/11/2025].

Yukon Geological Survey, 2023. Yukon Digital Bedrock Geology. Yukon Geological Survey, http://datatest.geology.gov.yk.ca/Compilation/3, [accessed 22/10/2025].